2001

Positron Annihilation Spectroscopy Study of Interfacial Defects Formed by Dissolution of Aluminum in Aqueous Sodium Hydroxide

Kurt R. Hebert
Iowa State University, krhebert@iastate.edu

Huiquan Wu
Iowa State University

Thomas Gessman
Washington State University

See next page for additional authors

Positron Annihilation Spectroscopy Study of Interfacial Defects Formed by Dissolution of Aluminum in Aqueous Sodium Hydroxide

Abstract
High-purity aluminum foils were examined using positron annihilation spectroscopy (PAS) after dissolution for various times in 1 M NaOH at room temperature. Measurements of the *S* and *W* shape parameters of the annihilation photopeak at 511 keV show the presence of voids of at least nanometer dimension located at the metal-oxide film interface. The large *S*parameter suggests that the metallic surface of the void is free of oxide. Voids are found in as-received foils and are also produced by dissolution in NaOH, evidently by a solid-state interfacial process. Atomic force microscopy (AFM) images of NaOH-dissolved foils, after stripping the surface oxide film in chromic-phosphoric acid bath, reveal cavities on the order of 100 nm size. The average cavity depth is in quantitative agreement with the PAS-derived thickness of the interfacial void-containing layer, and the dissolution time dependence of the defect layer *S* parameter closely parallels that of the fractional coverage of the foil surface by cavities; thus, the cavities are believed to be interfacial voids created along with those detected by PAS. The cavity distribution on the surface closely resembles that of corrosion pits formed by anodic etching in 1 M HCl, thereby suggesting that the interfacial voids revealed by AFM serve as sites for pit initiation.

Keywords
sodium compounds, dissolving, aluminum, interface structure, point defects, voids (solid), positron annihilation

Disciplines
Chemical Engineering

Comments
This article is from *Journal of the Electrochemical Society* 148 (2001): B92–B100, doi:10.1149/1.1341241. Posted with permission.

Authors
Kurt R. Hebert, Huiquan Wu, Thomas Gessman, and Kelvin Lynn

Journal of The Electrochemical Society, **148** (2) B92-B100 (2001)
0013-4651/2001/148(2)/B92/9/$7.00 © The Electrochemical Society, Inc.

Positron Annihilation Spectroscopy Study of Interfacial Defects Formed by Dissolution of Aluminum in Aqueous Sodium Hydroxide

Kurt R. Hebert,[a,*,z] Huiquan Wu,[a,] Thomas Gessmann,[b] and Kelvin Lynn[b]**

[a]*Department of Chemical Engineering, Iowa State University, Ames, Iowa 50011, USA*
[b]*Department of Physics, Washington State University, Pullman, Washington 99164, USA*

High-purity aluminum foils were examined using positron annihilation spectroscopy (PAS) after dissolution for various times in 1 M NaOH at room temperature. Measurements of the *S* and *W* shape parameters of the annihilation photopeak at 511 keV show the presence of voids of at least nanometer dimension located at the metal-oxide film interface. The large *S* parameter suggests that the metallic surface of the void is free of oxide. Voids are found in as-received foils and are also produced by dissolution in NaOH, evidently by a solid-state interfacial process. Atomic force microscopy (AFM) images of NaOH-dissolved foils, after stripping the surface oxide film in chromic-phosphoric acid bath, reveal cavities on the order of 100 nm size. The average cavity depth is in quantitative agreement with the PAS-derived thickness of the interfacial void-containing layer, and the dissolution time dependence of the defect layer *S* parameter closely parallels that of the fractional coverage of the foil surface by cavities; thus, the cavities are believed to be interfacial voids created along with those detected by PAS. The cavity distribution on the surface closely resembles that of corrosion pits formed by anodic etching in 1 M HCl, thereby suggesting that the interfacial voids revealed by AFM serve as sites for pit initiation.
 [DOI: 10.1149/1.1341241]

Manuscript submitted March 9, 2000; revised manuscript received September 8, 2000.

In the production of electrolytic capacitors, high-purity aluminum foils are etched anodically in hot chloride solutions. Etching produces as many as $10^7/cm^2$ etch pits on the foil surface, resulting in large increases in the foil's surface area and capacitance. The thermomechanical processing of these foils, as well as the use of surface pretreatments before etching, are optimized to promote the formation of large numbers of evenly spaced pits. The pretreatment baths are typically caustic or acidic solutions in which surface dissolution occurs. Improved understanding of the pitting sites would enhance the capability to engineer the etching process. Also, since pitting during etching and corrosion are fundamentally the same, this understanding would be of direct interest from the broader perspective of controlling pitting corrosion. While progress in recent years has been made in the detection of pit precursor sites on alloys, these sites are frequently related to second-phase particles which have no direct counterpart in high-purity aluminum. The precursor sites on pure metals may be too small to be detected using the same techniques which have been applied with success to alloy systems.

Positron-based techniques such as positron annihilation spectroscopy (PAS) are specifically sensitive to atomic-scale open-volume defects such as vacancies, vacancy clusters, and microvoids, and have been widely used to detect these defects in metals, alloys, semiconductors, and ceramic materials. They have been used in electronic materials processing applications, such as those involving thin surface films which are similar in dimension and geometry to oxide-film-coated passive metals.[1-3] Wu *et al.* and Fomino *et al.* previously used Doppler-broadening PAS to investigate high-purity aluminum capacitor foils.[4,5] Wu found significant numbers of defects near the metal-oxide film interface, and observed that the number of defects or their size increased due to open-circuit dissolution in NaOH solution. The same dissolution process enhances the number of pitting sites when used as a pretreatment for etching. The present work was conducted to explore the fundamental connection between the PAS-detected defects and pit sites. The effect of dissolution time on PAS measurements was investigated, and the results are compared to atomic force microscopy (AFM) images of foils dissolved for the same times, in which the surface oxide film is dissolved to reveal defects.

Experimental

The aluminum samples are 99.98% purity annealed foils, about 100 μm thick with a typical grain size of 100 μm (provided by KDK Corporation). Solutions were prepared from reagent grade chemicals and distilled and deionized water. Dissolution in 1 M NaOH was carried out at open circuit and room temperature. Positron measurements were conducted in a vacuum chamber at a pressure of about 10^{-7} Torr. A monoenergetic positron beam was produced by the ^{22}Na source in the chamber. The beam implanted positrons within the sample at a mean depth given by

$$z_m = 14.8E_b^{1.6} \quad [1]$$

where the mean depth z_m is in units of nanometers and the beam energy E_b is in kiloelectronvolts.[1] Spectra were compiled at typically 60 values of the beam energy ranging from 0.03 to 20 keV. At each energy, a Doppler-broadened gamma radiation spectrum was measured using a Ge detector mounted perpendicular to the beam direction. Each spectrum consisted of about 1×10^6 photon counts, with 6×10^5 counts in the annihilation photopeak around 511 keV. *S* and *W* parameters were calculated by the system software, to within an accuracy of 0.001. Further details of slow positron beam system characteristics are given by Lynn and Lutz.[6]

AFM examination of the foil surfaces was carried out in air, using a 14 μm scanner along with Si cantilevers and a silicon nitride tip (Digital Instruments Nanoscope III). Analysis of the areas of cavities formed by dissolution was carried out using the Image SXM software application. Prior to AFM observation, some NaOH treated foils were placed in solutions of chromic-phosphoric acid, in order to dissolve the surface oxide film. The chromic-phosphoric acid bath consisted of 2 wt % CrO_3 and 2 wt % H_3PO_4 at 85°C, and the immersion time of foils in it was typically 1 min. Additionally, the open-circuit potential transients during dissolution in NaOH were measured using a high speed voltmeter (Keithley 194A) interfaced to a personal computer, in order to ascertain changes in the oxide film thickness resulting from caustic immersion. Anodic etching was carried out at a constant applied current density of 0.3 A/cm^2, in a mixed bath of 6 NH_2SO_4 and 1 M HCl, at 90°C, for a period of 5 s. A potentiostat/galvanostat (EG&G PAR 273) was used to deliver the etching current.

* Electrochemical Society Active Member.
** Electrochemical Society Student Member.
z E-mail: krhebert@iastate.edu

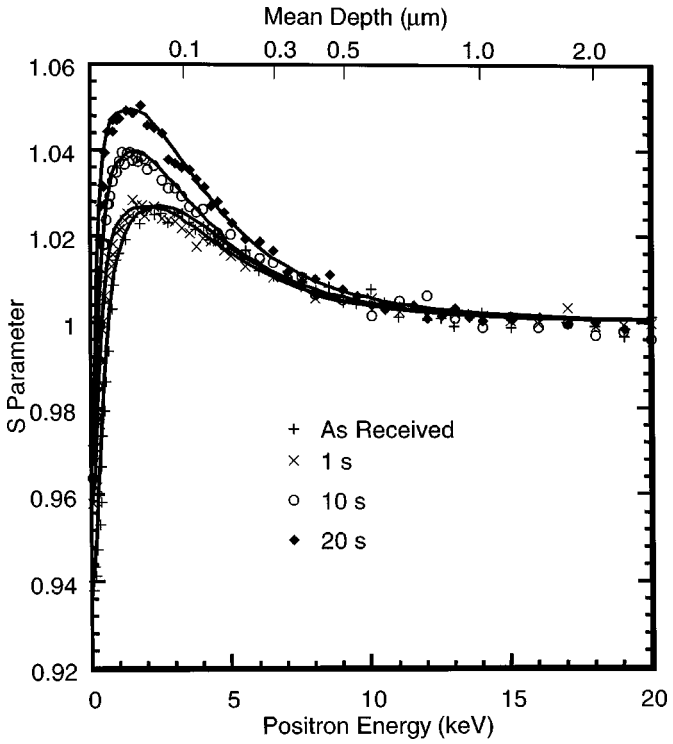

Figure 1. *S* energy profiles of as-received aluminum foil, and after dissolution in NaOH for 1, 10, and 20 s. Data points are measured values, and solid lines are results of fitting with simulation. Top scale is mean implantation depth according to Eq. 1.

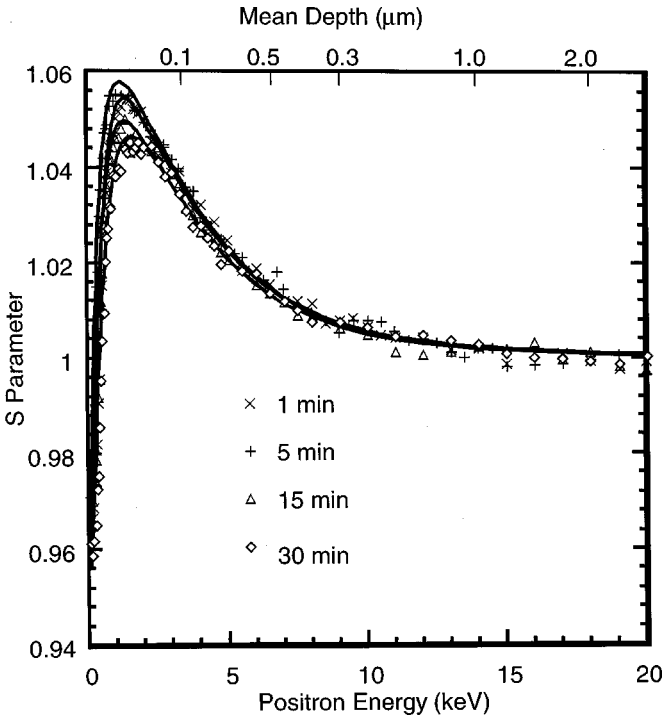

Figure 2. *S* energy profiles of foils after dissolution for 1, 5, 15, and 30 min. Data points are measured values, and solid lines are results of fitting with the simulation. Top scale is mean implantation depth from Eq. 1.

Results and Discussion

PAS measurements.—Once implanted, positrons thermalize rapidly and then diffuse within the solid for a period on the order of several hundred picoseconds, after which they are either directly annihilated by electrons, or else ''trapped'' into open volume defects. Trapping is the result of the electrostatic attraction between positrons and these defects, which are negative charge centers due to the penetration into the defect of the valence electrons of neighboring atoms. Positrons trapped in defects eventually annihilate with these valence electrons. Annihilation, whether it occurs in defects or elsewhere, converts the combined mass of the positron and electron into the energy of gamma photons. For the typical case of two photons produced, the photon energy equivalent to the particle masses is 511 keV (*i.e.*, mc^2). However, the photon energies do not have this specific value but instead are distributed about it in a photopeak; the energy displacement from 511 keV is due to a Doppler shift associated with the photon momentum. Since annihilation conserves momentum, the extent of the shift is determined by the momentum of the annihilating electron (the positron momentum being very small). Hence, the peak shape is a direct indication of the local momentum distribution of electrons involved in annihilation. Annihilation in defects occurs predominantly by relatively slow-moving valence electrons; thus, defective regions of the metal are characterized by narrow photopeaks. On the other hand, photopeaks in defect-free regions are broader because of the participation of faster-moving core electrons, as well as valence electrons, in annihilation.

In this work, the shape of the primary annihilation photopeak at 511 keV was characterized by the parameters *S* (the ratio of the central peak area to its total area, related to annihilation by valence electrons), and *W* (the ratio of the ''tail'' area of the photopeak to its total area, associated with core electrons). The presence of open-volume defects can be inferred from relatively large values of *S* and small values of *W*. Figure 1 shows the *S* parameter measurements of an aluminum foil in the as-received condition, and after dissolution in NaOH for times up to 20 s. The positron beam energy on the horizontal axis determines the mean implantation depth, according to Eq. 1. In the figure, the data points are calculated from individual experimental spectra, while the solid line is the result of a simulation, to be explained below. The estimated accuracy of the experimental *S* values is within 0.001. The *S* values in this paper are normalized by dividing by the bulk *S* parameter, which in Fig. 1 is approached as a plateau at energy greater than 15 keV. Since the foils are annealed with a large grain size of 100 μm, the bulk metal has a very small vacancy concentration and serves as a defect-free reference state. With the normalization, *S* values larger than one indicate the presence either of phases having *S* parameters larger than aluminum, or else open volume defects. The profiles in Fig. 1 show that in each foil there are regions extending to depths on the order of 100 nm from the surface which have characteristic *S* parameters larger than 1. The oxide layer thickness on the as-received foil was found to be 5 nm from Auger measurements,[9] and it is shown below that the NaOH treatment reduces the film thickness. Therefore, since oxide thickness is much smaller than 100 nm, the high *S* regions are defect-containing layers in the metal beneath the metal-film interface. Figure 1 shows that the as-received foil contains these near-surface defects, and that changes in the defect distribution occur due to NaOH treatment. Figure 2 shows additional *S* energy measurements at longer dissolution times. The *S* and *W* parameter measurements for all dissolution times were highly reproducible.

Information about the types of defects is revealed by plotting the *S* parameter *vs.* the *W* parameter, as shown in Fig. 3. The data for all the experiments are displayed in Fig. 3, which does not show the energy explicitly. *S* and *W* values for individual experiments fall on a common locus, which consists of two straight line segments connecting three vertices. As the energy is increased, points move along the top segment from left to right, reach a maximum *S* value, and then move along the bottom segment from right to left. The vertices correspond to states with defined values of *S* and *W*, which can be phases such as the metal or oxide, or else particular kinds of defects.

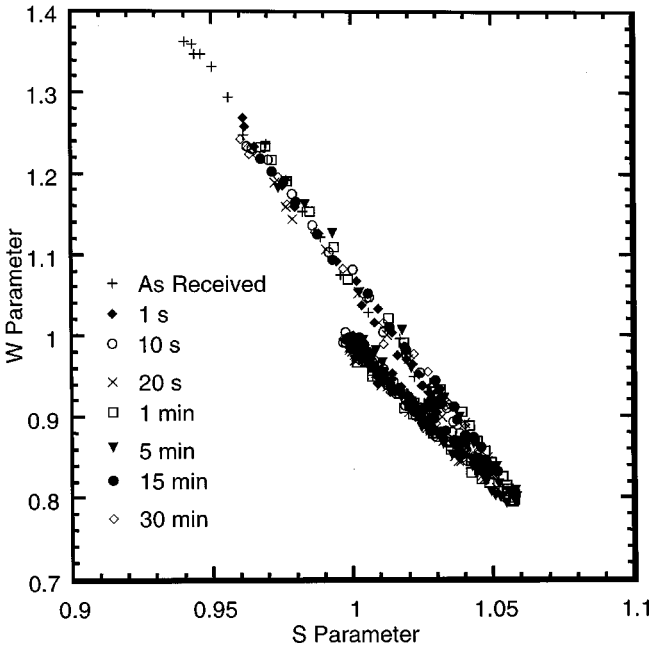

Figure 3. Plot of experimental *W* and *S* parameters for as-received foil and for all dissolution times. *W* and *S* are normalized with respect to their values for the bulk metal.

The end point at low energy is marked by a cluster of points for the as-received foil, at *S* of 0.94 and *W* of 1.36. Previously, Fomino found comparable *S* values of 0.92 for 50 and 100 V anodic oxide layers formed in borate buffer, and 0.93 for the thick, possibly porous, oxide layers produced by electropolishing aluminum in phosphoric acid-ethanol-water baths.[7] Van Hoecke *et al.* measured *S* parameters of 0.93 near the surface of porous anodic films grown in phosphoric and sulfuric acid.[8] The maximum beam energy in the low *S* cluster is 0.138 keV, corresponding to z_m of 0.62 nm from Eq. 1. Since this depth is significantly smaller than the 5 nm oxide thickness on the as-received foil, the positrons at these low energies would be implanted in the oxide layer. Therefore, the low-energy *S*-*W* state represents annihilation of positrons trapped in the amorphous oxide film. The *S*-*W* points of foils subjected to NaOH treatments do not approach this state at the lowest beam energy, because their oxide layer thickness are reduced by dissolution. The other *S*-*W* states in Fig. 3 represent bulk defect-free aluminum ($S = 1.00$, $W = 1.00$), and the open volume defect near the metal-oxide interface ($S = 1.06$, $W = 0.80$).

The interpretation of straight line segments in *S*-*W* plots is explained by Hautojärvi and Corbel.[3] Assuming that that only two states (defect and nondefect) contribute to annihilation, the measured *S* and *W* represent a superposition of these states

$$S = (1 - x_D)S_B + x_D S_D$$

$$W = (1 - x_D)W_B + x_D W_D \qquad [2]$$

where S_D and W_D are the parameters of the defect state (*i.e.*, 1.06 and 0.80), S_B and W_B those of the nondefect state, and x_D is the fraction of positrons which are trapped into defects. x_D is energy-dependent, increasing from 0 to 1 with increasing energy along the oxide-defect line, and decreasing from 1 to 0 with energy along the defect-bulk metal line. Eliminating x_D between these equations results in a linear equation relating *S* and *W*

$$\frac{W - W_B}{S - S_B} = \frac{W_D - W_B}{S_D - S_B} \qquad [3]$$

Thus, the straight line segments indicate that only two states contribute to annihilation. For most of the experiments in Fig. 3, Eq. 3 is followed except near the maximum *S*, where the *S*-*W* locus curves below the oxide-defect line to join the defect-bulk line. S_D and W_D are not closely approached except by the 1 and 5 min dissolution experiments. However, even though data for a given experiment may never reach these values, Eq. 3 indicates that the parameters of the defect contributing to annihilation are S_D and W_D. Therefore, Fig. 3 shows that only one defect type is present in all the measurements, on as-received foil as well as NaOH treated foils. The curvature near the maximum *S* in many experiments is caused by relatively small concentrations of this defect, so that all three states contribute to annihilation.

Information about the defect size is conveyed by its *S* and *W* parameters. *S* typically increases and *W* decreases as the defect size becomes larger, as measurements on silicon demonstrate.[10] Schultz and Lynn found the *S* parameter of vacancies in aluminum to be 1.027.[11] The present *S* of 1.06 is significantly larger than this value, and approaches the *S* of 1.10 obtained by Huomo *et al.* for the unfilmed Al(110) surface at 400 K.[12] As pointed out by van Veen *et al.*, *S* values around 1.10 are explained by the presence of positronium (Ps), an electron-positron bound state which can be formed in cavities at least 0.8 nm in size or at surfaces.[13] On open surfaces, Ps decays by a combination of two-photon annihilation (*para*-Ps) at energies very close to maximum of the 511 keV photopeak, and three-photon annihilation (*ortho*-Ps) at energies away from the photopeak. Unlike Huomo's measurements on clean aluminum surfaces, the present spectra show no evidence of enhanced off-peak annihilation in the defect layer, due to *ortho*-Ps. However, in voids, *ortho*-Ps frequently undergoes ''pick-off'' annihilation with the electrons of the surrounding solid atoms, producing photons at energies in the photopeak but not necessarily close to the maximum.[13] The resulting *S* parameter for voids is large due to the sharp peak contributed by *para*-Ps decay. Thus, the expected annihilation characteristics of voids, namely, large *S* values and no three-photon annihilation, are those of the defects found in the present measurements. It can be inferred that these defects are voids of at least nanometer size.

As mentioned earlier, the low *S* of 0.94 for the surface oxide film is the result of annihilation of positrons trapped within the oxide. If a similar oxide were present on the internal surface of voids, a low *S* would also be expected for the voids. The observed high *S* value of 1.06, then, contradicts the presence of such a film on the void surface. Any oxide on the voids would necessarily be very thin (approximately one monolayer) so that it does not effectively trap positrons.[14] If during the formation of a void its surface had been exposed to air or aqueous solution, it would have oxidized and formed a film like that on the external surface. Hence, the absence of such a film indicates that the voids form by a solid-state process, and not by dissolution. As discussed below, if the void surface is either oxide-free or else covered by a very thin, nonprotective oxide, it can function effectively as a pit initiation site, in media where dissolution of the overlying material can occur. Near-surface voids with clean metal surfaces then have significant implications for corrosion phenomena.

Simulation of PAS mMeasurements.—*S*-energy measurements cannot be interpreted directly as depth profiles of defect concentration, since annihilation does not generally occur at the precise depth indicated by Eq. 1 and the top axis in Fig. 1 and 2. The reasons are that (*i*) at a given beam energy, the implantation depths are spread about the mean depth, and (*ii*) positrons may diffuse to a different depth during the time between implantation and annihilation. Therefore, positrons implanted at energies corresponding to the defect-containing region, for example, may annihilate outside this region. Quantitative analysis of the spatial distribution of defects requires fitting the *S* profiles to a solution of the diffusion-annihilation equation for positrons in a solid. This equation is a differential balance on positrons in the solid, and accounts for diffusion and implanta-

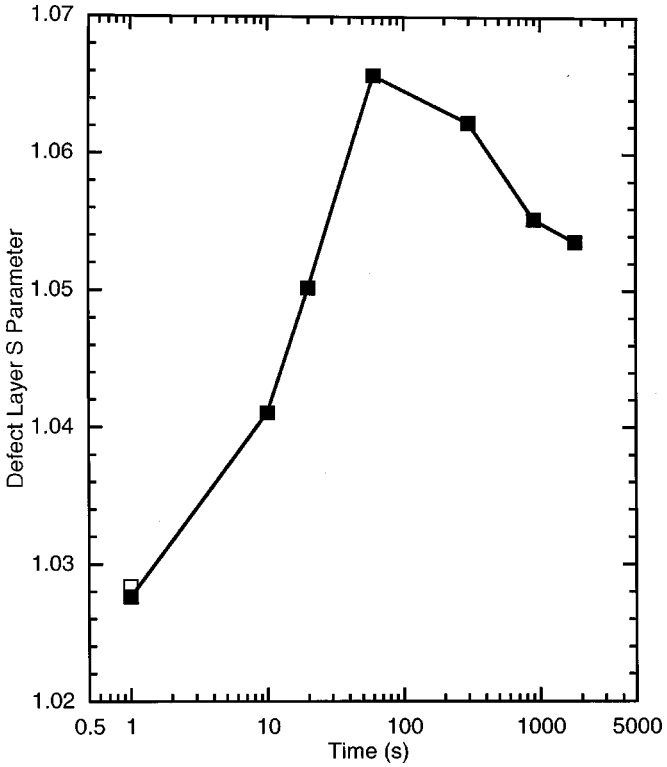

Figure 4. Model defect layer *S* parameter *vs.* dissolution time. Open square is for as-received foil.

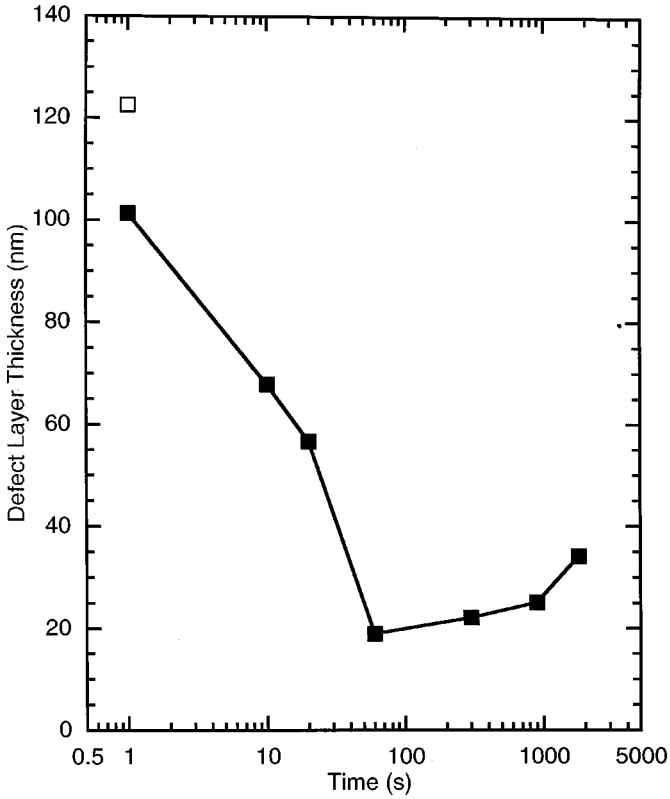

Figure 5. Model defect layer thickness fit *vs.* dissolution time. Open square is for as-received foil.

tion of positrons, and their removal by either annihilation or trapping into defects.[1] The local trapping rate is determined by the concentration profile of defects specific to a given sample. Solution of the diffusion-annihilation equation was accomplished using VEPFIT, a software application written for that purpose.[15,16] VEPFIT uses the positron concentration profile to calculate the *S*-energy profile, and fits the parameters of the defect distribution to obtain agreement with the experimental *S* measurements.

In this work, the distribution of phases and defects in the samples in simulations are approximated by simple layer models, in which each layer has a uniform *S* parameter, thickness, and positron diffusion length. The latter parameter represents the mean distance which positrons diffuse before they are either annihilated or trapped by defects. The models used for fitting contain a surface defect layer and a bulk aluminum layer. Inclusion of the oxide layer was found to be unnecessary, as the oxide is so thin that the defect layer parameters obtained by the simulation are unaffected by its presence, even when the oxide diffusion length is set to very low values. Thus, the oxide film factors into the model as a surface boundary condition. The only input parameter for the simulation is the bulk aluminum diffusion length, which is set to 150 nm, consistent with literature values of the positron diffusion coefficient and bulk lifetime.[1,17] The quality of the model fit to the experimental *S*-energy profiles is very good, as indicated by the proximity to the data of the model curves in Fig. 1 and 2. The fit values of the defect layer *S* parameter, positron diffusion length, thickness are plotted in Fig. 4-6 *vs.* dissolution time. The parameters for the as-received foils are plotted at times of 1 s on the logarithmic time axis, using open symbols.

Figure 4 shows that significant transient changes in the defect layer *S* parameter result from dissolution. The defect layer *S* parameters in Fig. 4 in most cases are smaller than S_D of 1.06, since annihilation in both defects themselves, as well as the nondefective solid in the defect layer, contribute to its value. S_d, the defect layer *S* parameter, is expressed as

$$S_d = f_D S_D + (1 - f_D) S_b \quad [4]$$

where S_b is unity, the *S* parameter of the perfect crystal, and f_D is the fraction of positrons trapped into defects themselves. The variation of S_d in Fig. 4 is due to changes in f_D, which is directly related to the void volume fraction in the defect layer. Hence, the void concentration increases up to 1 min, when nearly all the positrons annihilate in voids, and thereafter slowly declines. It can be noted from Fig. 1 and 2 that S_d is larger than the maxima of the *S* energy profiles. This is a consequence of implantation and diffusion of positrons into the bulk and surface layers, even when the mean depth from Eq. 1 is within the defect layer. Thus, the measurement includes energy-dependent contributions from annihilation in the bulk and surface states, which because of their relatively small *S* values cause the experimental *S* to be smaller than S_d.

The defect layer thickness in Fig. 5 decreases from 120 nm in the as-received foil to about 20 nm at 1 min. There is a significant drop in the defect layer thickness in the first 1 s in NaOH. Since the foil dissolves at a rate of approximately 200 nm/min in the caustic bath,[9] the time needed to remove the original defect layer by dissolution is approximately 1 min. Hence, the decrease in the defect layer thickness in 1 min represents a transition from the relatively thick defect layer on the as-received foil to a layer having a smaller characteristic thickness of 20 nm, containing new voids created by dissolution. During the course of dissolution, voids present at a given time would be quickly removed as the surrounding metal dissolved. The declining S_d at long times in Fig. 4 then suggests that defects continue to form at these times, but do so at a smaller rate compared to their removal by dissolution. As argued above, the large S_D value suggests that this void formation occurs by a solid-state process and not by dissolution itself. The relation between the defect layer thickness and defect size is considered in detailed fashion after the AFM results are presented.

According to Fig. 6, the positron diffusion length is 5.4 nm for the as-received foil, drops abruptly to 3.2 nm in the first second of dissolution, decreases further to 1.6 nm at 20 s, and eventually in-

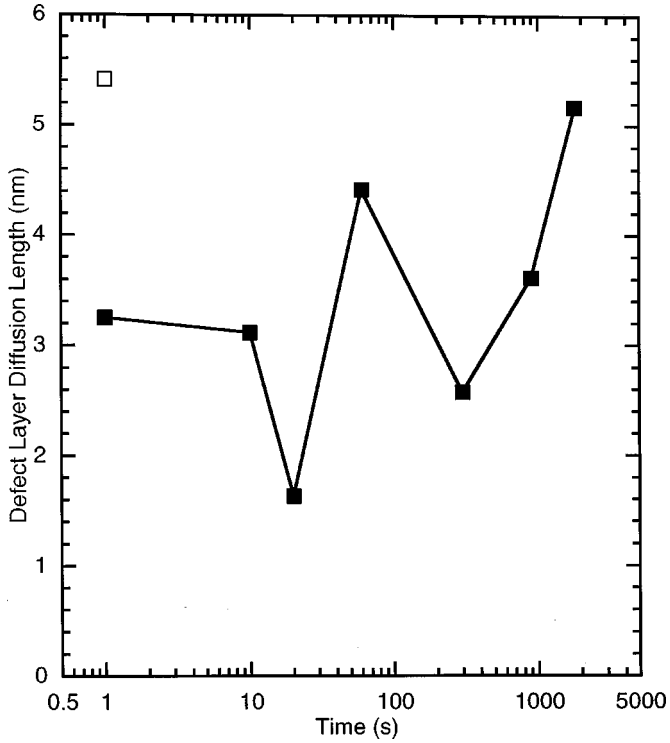

Figure 6. Model defect layer positron diffusion length *vs.* dissolution time. Open square is for as-received foil.

creases to 5.2 nm at 30 min. The defect layer diffusion length is related to the void concentration and to the rate constant for trapping into voids. The relationship of the defect concentration C and the defect layer diffusion length L_d is

$$C = \left[\left(\frac{L_b}{L_d}\right)^2 - 1\right]\frac{1}{\nu\tau_b} \qquad [5]$$

where L_b is 150 nm, the diffusion length in the bulk aluminum, ν is the trapping rate constant, and τ_b is the positron lifetime in bulk aluminum, 162 ps.[17] The trapping rate constant depends strongly on the unknown defect size.[3] Thus, Eq. 5 cannot be used to obtain a useful estimate of the concentration. However, since L_d is 30-90 times smaller than L_b, it is clear that the near-surface region is highly defective in all the samples. Also, the drop in L_d in the first moments of dissolution suggest production of defects, as has been inferred above from the behavior of the defect layer S parameter and thickness.

While the model defect layer analysis is not sensitive to the presence of the oxide layer, evidence for the oxide can be obtained from the *S*-*W* plot. The low energy branch of the *S*-*W* locus represents the range of energy for which the oxide contributes significantly to annihilation. The highest energy on this branch corresponds to a depth at which positrons are implanted in the defect layer, but have a high probability of diffusing into the oxide. Hence, the oxide thickness was estimated by subtracting the defect layer diffusion length from the depth found from Eq. 1. The resulting thickness is 9 nm for the as-received foil, and between 3 and 7 nm for the samples dissolved in NaOH. While this estimate for the as-received sample is somewhat higher than the Auger-determined thickness of 5 nm,[9] the calculated thickness is on the correct order of magnitude, and decreases as expected due to the NaOH treatment. Therefore, the calculation confirms the presence of the oxide over the defect layer, further demonstrating that the defects are located at or close to the metal-film interface.

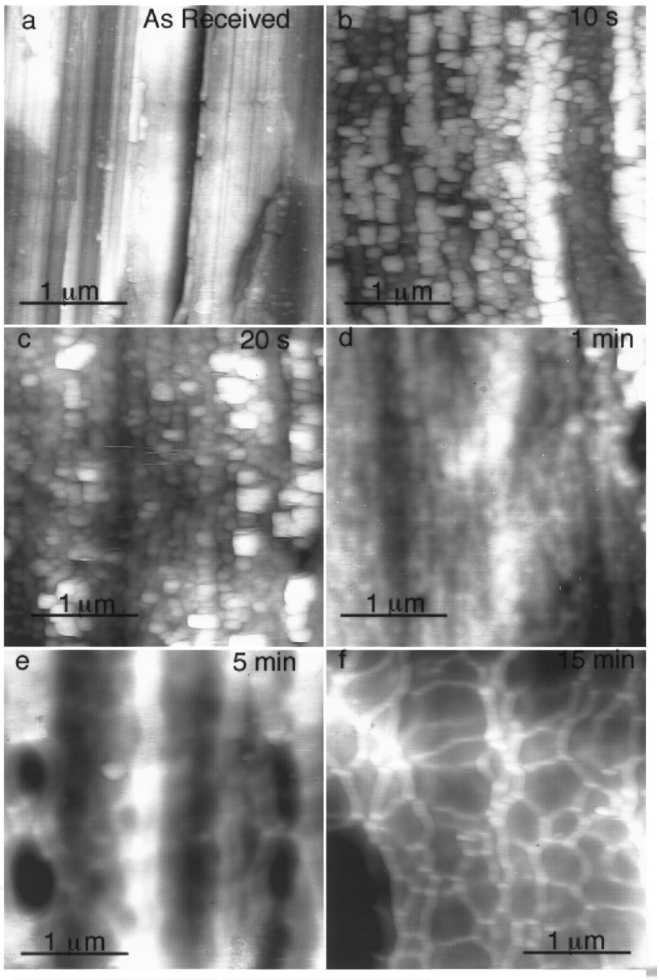

Figure 7. Top view AFM images after dissolution of foils in 1 M NaOH for various times: (a) as-received, height contrast 90 nm; (b) dissolution time 10 s, height contrast 80 nm; (c) 20 s, 111 nm; (d) 1 min, 85 nm; (e) 5 min, 80 nm; (f) 15 min, 105 nm.

AFM topographic images during dissolution.—AFM was used to follow changes in surface topography during dissolution in NaOH. Figure 7 shows a series of 3 × 3 μm top view images at different dissolution times. The surface of the as-received foil (Fig. 7a) contains many ridges several tenths of micrometer wide. This topography is typical of other high-purity aluminum foils.[18] The change in surface appearance due to 1 s dissolution is not evident in top view images, but can be appreciated in the illuminate view images in Fig. 8. These images are the result of application of a type of high-pass filter which highlights features smaller than about the order of 100 nm but suppresses micrometer-scale topography. Figure 8 shows that dissolution for 1 s preferentially removes many narrow ridges and asperities smaller than 100 nm in width. The 10 s image in Fig. 7 shows the appearance of many 100-200 nm wide particle-like features, which at 20 s appear to completely cover the surface. Martin and Hebert showed evidence from Auger spectroscopy that these particles are formed at small ''hills'' on the as-received foils where the oxide film is a few nanometers thicker than elsewhere.[19] Since this thicker oxide partially inhibits dissolution in NaOH, the surrounding area dissolves preferentially, giving the hill the appearance of a particle after dissolution. No evidence of the particles is seen at 1 min, possibly because they are undercut by dissolution and removed. At this time, the ridge texture of the as-received foil is only faintly visible, as dissolution has continued to remove larger and larger ridges. The 5 and 15 min images reveal the initiation of a new

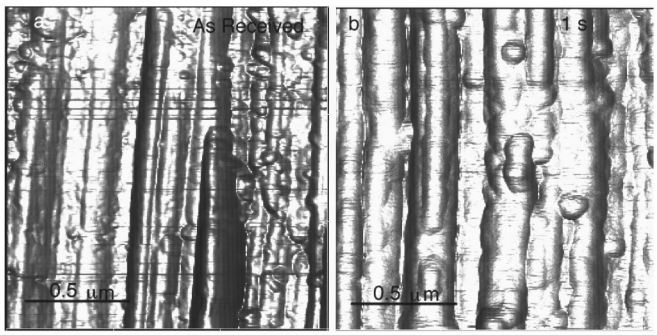

Figure 8. Illuminate view images comparing foil surface (a) as-received and (b) after 1 s dissolution.

topographic texture associated with dissolution itself, which consists of scalloped depressions several hundred of nanometer in width, which are surrounded by ridges. The appearance of the foil surface after 30 min dissolution (not shown) is also dominated by the scallop texture. The scallop topography is found on aluminum after other dissolution processes as well.[20,21]

As mentioned above, the defects are at least of nanometer dimensions, which suggests the possibility of viewing them with AFM after the overlaying surface oxide is dissolved. Accordingly, a series of experiments was performed in which, after dissolution in NaOH, the foils were immersed in a solution of 2 wt % CrO_3 and 5 wt % H_3PO_4 at 85°C in order to strip the oxide film. This chromic-phosphoric acid treatment uniformly dissolves the oxide layer, eventually replacing it with a thin chromium oxide passivating film which is believed to suppress metal oxidation. Stripping was carried out for times of 60-150 s, the time being increased as needed to reveal small cavities on the surface. AFM images of foils subjected to the stripping treatment after dissolution for various times in NaOH are shown in Fig. 9 and 10. All these images represent the foil surface for the earliest stripping time at which the cavities appear. The surface of the as-received foil (Fig. 9a) has both small isolated cavities as well as larger elongated ones distributed along ridges. The images after 10 s to 1 min in NaOH (Fig. 9b-d) reveal an increasingly roughened surface with escalating numbers of 100 nm scale cavities, which eventually at 1 min appear to form an interconnected network. In the 20 s image, the oxide stripping treatment causes the particles found in Fig. 7c to largely disappear. Since particles are believed to be metallic features, this suggests that a small extent of metal dissolution can occur in the stripping bath, even though no weight loss could be detected after dissolution times of tens of minutes.

From 5 to 30 min (Fig. 10), the cavities are isolated and distinct from the relatively smooth surrounding surface, and are found at the bottom of the depressions between the ridges. After 1 min, the cavity number density decreases with time. Both Fig. 9 and 10 show that the topography of the stripped surface depends markedly on dissolution time in NaOH. With increasing time in the chromic-phosphoric acid bath, individual cavities are enlarged by dissolution, while the microscopic texture of the surrounding surface does not change. Apparently, the cavities function as localized dissolution sites in the stripping solution, while dissolution on the surrounding surface proceeds comparatively much more slowly.

The cavities in Fig. 9 and 10 are either corrosion pits which initiate in the stripping solution (presumably at oxide defects formed during NaOH treatment), or else interfacial voids formed in NaOH, and exposed by oxide stripping. To explore the relationship of the cavities to PAS-detected voids, the cavity geometry and distribution are compared with model defect layer parameters. Figure 11 compares the average cavity depth and the model defect layer thickness as a function of NaOH dissolution time, and shows that the two measurements are quantitatively comparable at each time. The cavity depth, like the defect layer thickness, decreases from an initial value of about 130 nm for the as-received foil to less than 40 nm after 1 min. The small discrepancy between the depths and the defect layer thickness of about 20 nm is possibly due to dissolution from the cavities in the stripping solution. As discussed above,

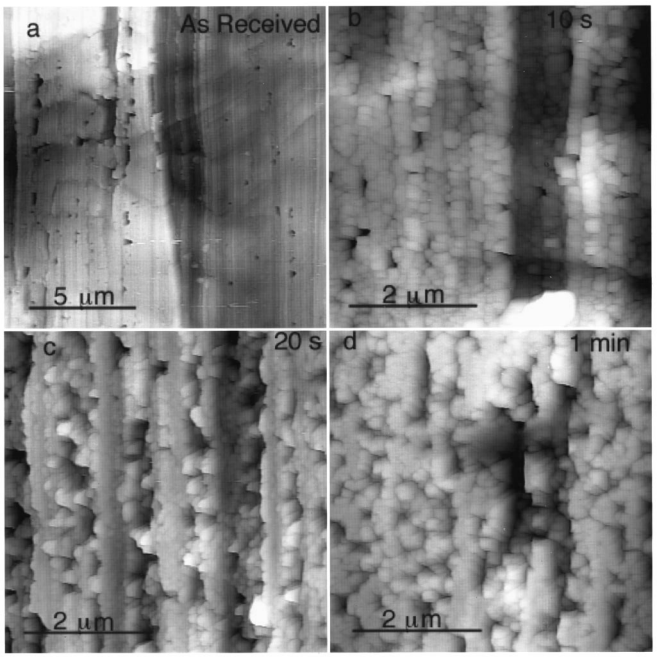

Figure 9. Top view AFM images after dissolution of foils in 1 M NaOH for various times, followed by oxide film stripping in chromic-phosphoric acid bath. (a) As-received, stripping time 1.5 min, height contrast 440 nm; (b) 10 s in NaOH, stripping time 2.5 min, 151 nm; (c) 20 s in NaOH, stripping time 1.5 min, 270 nm; (d) 1 min in NaOH, stripping time 1.5 min, 270 nm.

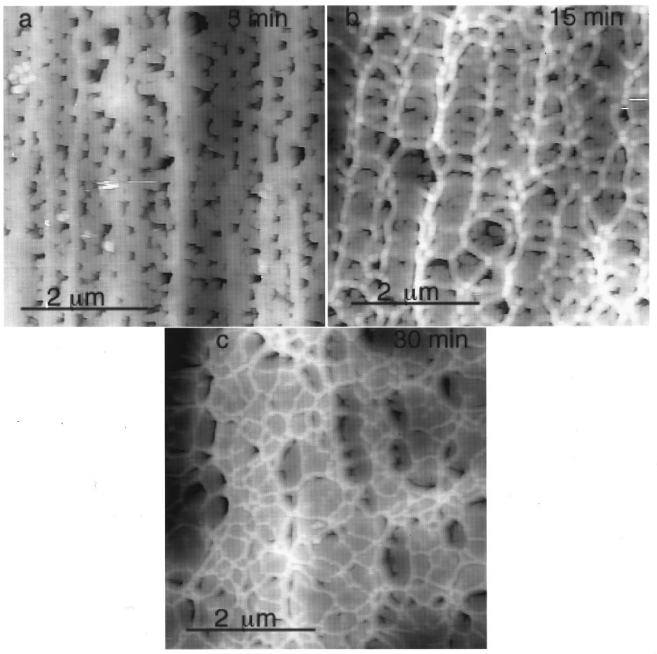

Figure 10. Top view AFM images after dissolution of foils in 1 M NaOH for various times, followed by oxide film stripping time for 1 min in chromic-phosphoric acid bath. (a) 5 min in NaOH, height contrast 162 nm; (b) 15 min in NaOH, 100 nm; (c) 30 min in NaOH, 176 nm.

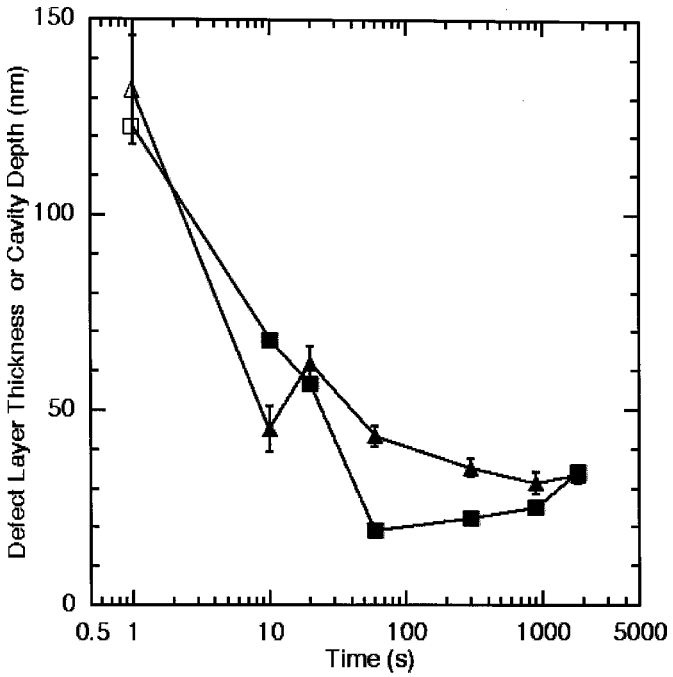

Figure 11. Comparison of model defect layer thickness (from Fig. 5) and mean cavity depth from AFM images of foils treated in NaOH followed by stripping oxide film in chromic-phosphoric acid. Error bars denote 90% confidence intervals based on measurement of between 25 and 50 cavities.

changes in the model defect layer *S* parameter (S_d) with dissolution time are considered to at least qualitatively reflect variations of the void volume fraction in the defect layer, which should be equivalent to the fractional surface area intercepted by the voids. Accordingly, the fractional coverage of the foil surface with cavities was also determined from the AFM images, and is compared to S_d in Fig. 12.

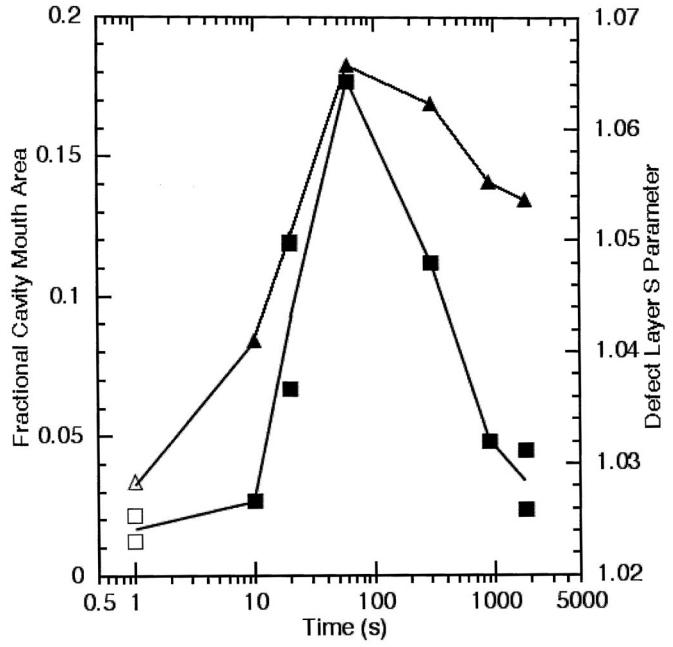

Figure 12. Comparison of model defect layer *S* parameter (from Fig. 4) and the fractional coverage of the foil surface with cavities, the latter estimated using AFM image analysis.

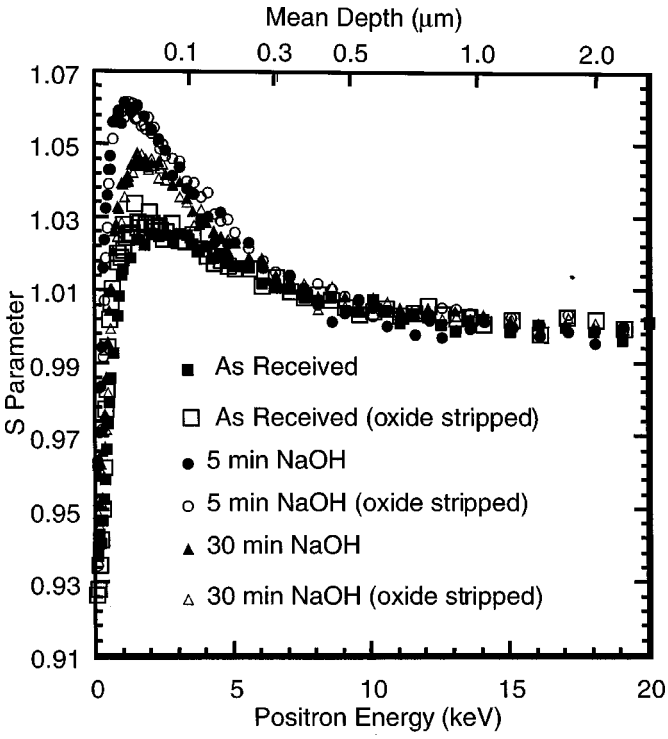

Figure 13. Effect of chromic-phosphoric acid oxide stripping treatment on *S* energy profiles. Open and closed symbols are for foils before and after oxide stripping treatment. Immersion times in stripping bath are as-received, 1.5 min; 5 min NaOH, 1 min; 30 min NaOH, 1 min.

This comparison reveals that both measurements show a consistent time dependence, in which they increase to a maximum at 1 min and then decline.

Figures 11 and 12 show that the defect layer properties found by PAS are equivalent to the geometric characteristics of the cavities revealed by stripping. One explanation for this correspondence is simply that the cavities are interfacial voids exposed by dissolution in the stripping solution. To assess this possibility, an additional set of positron measurements was carried out after the same oxide stripping treatments in Fig. 9 and 10. Exposure of the void surface to aqueous solution by stripping the oxide film should cause this surface to oxidize. Thus, if stripping reveals all the voids, the peak in the *S* energy plots would disappear since the defect layer *S* parameter would be reduced to a low value of 0.92-0.94 characteristic of positrons trapped in oxide layers. Figure 13 compares *S* energy profiles before and after oxide stripping for as-received foils, and foils treated in NaOH for 5 and 30 min. It is clear that for each case, there is no significant change in the *S* parameter of the voids due to oxide stripping. This implies that the cavities in Fig. 9 and 10 are not the interfacial voids detected by positrons. The true voids contributing to the high *S* parameter are not revealed by oxide stripping, and may be located somewhat below the metal-oxide interface. However, the strong correspondence with AFM shows that the thickness of the void-containing layer is similar to the cavity depths, and the surface coverage of cavities is directly related to the volume fraction of voids. Therefore the cavities and voids are correlated, perhaps forming as a result of the same process.

An explanation for the ''hidden'' defects may be found in the AFM study of Martin and Hebert, who investigated NaOH treatment of different high-purity aluminum foils from the one used in this work.[19] After 20 s NaOH immersion, a foil was viewed while at the same time dissolving in 1 M H_2SO_4. Unlike the chromic-phosphoric acid oxide stripping bath, aluminum metal dissolves continuously in this solution at a rate on the order of 1 nm/min. The images revealed two distinct kinds of cavities which were exposed on the surface at

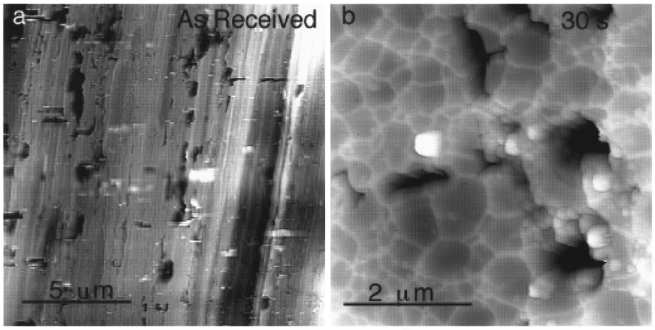

Figure 14. AFM images of foils etched in mixed 1 M HCl-6 M H_2SO_4 bath at 90°C for 5 s, at applied current density of 0.3 A/cm^2. (a) As-received foil used for etching, height contrast 440 nm. (b) Foil pretreated by 1 M NaOH immersion for 30 min, 500 nm.

different dissolution times: 100-200 nm wide cavities which appeared after about 15-20 min dissolution, and more numerous cavities significantly smaller than 100 nm in width, seen at about 30-40 min. The large cavities were similar in morphology to the ones in Fig. 9. However, the small cavities, which are buried at depths of roughly 30-40 nm, would not have been exposed by the oxide stripping bath, and therefore may be the voids detected by positron measurements. Since the apparent distance of these voids below the surface is approximately the same as the depth of individual large cavities, the observed correlation between large cavity depth and defect layer thickness would be understandable.

Interfacial defects and etch pit sites.—In order to investigate the relationship of the voids to pitting sites, aluminum foils were anodically etched in the hydrochloric-sulfuric acid bath and then examined by AFM. Figure 14 shows images of the etched surfaces of both an as-received foil and one pretreated by 30 min dissolution in 1 M NaOH. Many of the pits on the as-received foil are elongated in the direction parallel to ridges, and are distributed in rows along these ridges. The shape of pits and their arrangement on the surface are similar to those of the cavities revealed by chromic-phosphoric acid dissolution (Fig. 9a). After 30 min dissolution in NaOH, pits are found to be either elongated in shape and positioned along the ridges of the scalloped surface texture, or else centered in the scallops, Again, the location and shape of pits clearly correspond to those of the cavities in Fig. 10c, which were exposed by dissolution in chromic-phosphoric acid.

As mentioned earlier, the cavities in Fig. 9 and 10 are interfacial voids located at or close to the metal-film interface. The positron measurements do not indicate whether the surface of these voids is oxidized, since their exposure by oxide stripping has no effect on the *S* parameter. If the surface has no protective oxide, initiation of metal dissolution would require only dissolution of the overlying oxide film, which is likely to occur in the highly acidic etchant bath. The observed correspondence between cavity and pit morphology would then be expected. On the other hand, if the void surfaces are covered with a several nanometer thick oxide layer, the initiation of pits at these sites would be difficult to understand. Therefore, it is suggested that at least a portion of the large interfacial voids revealed in Fig. 9 and 10 are either oxide-free, or at least do not have fully developed oxide layers on their surfaces, and these voids become pits during etching. These voids represent a small fraction of all the voids detected by positron measurements, the majority of which are buried deeper below the interface. This explains why exposure of the voids at the oxide-metal interface does not affect the *S* parameter.

Previously, Wiersma and Hebert used scanning electron microscopy to measure the volume of etch pits formed after anodic current pulses about 10 ms in length, in 1 M HCl at 70°C.[22] They found that the total volume of the submicrometer-size pits formed at these

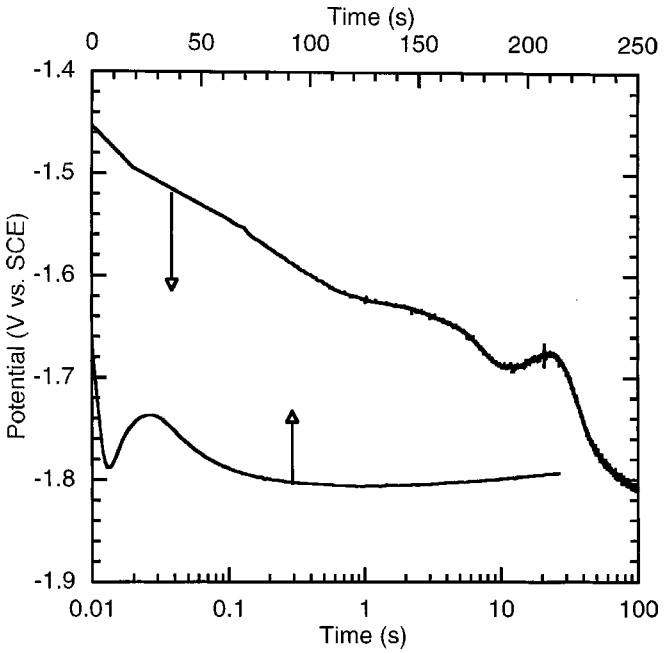

Figure 15. Potential transients during dissolution plotted to demonstrate both early- and long-time behavior.

small etch times exceeded by a factor of ten the faradaic equivalent volume of the charge passed. Thus, the pit volume could not be explained by anodic dissolution. The effective dissolution current density in these small pits, based on the pit depth and etching time, is very large, exceeding 100 A/cm^2. In view of the present results, both the excess pit volume and the high apparent current density may be explained by the view that a pit forms by oxide film dissolution above a pre-existing interfacial void. Hence, the ''anomalous initial pit growth'' actually occurs before etching, as the result of the solid-state process accounting for the growth of the interfacial void.

Surface oxide film dissolution.—The formation of interfacial voids during exposure to NaOH is possibly related to the high solubility and rapid dissolution of the oxide film in this solution. As mentioned earlier, the energy dependence of the *S* and *W* parameters was used to estimate the surface oxide thickness. The surface oxides on foils treated in NaOH for 1 s or more were found to be at least 2 nm thinner than the film on the as-received foil. This calculation suggests that rapid partial dissolution of the film occurs upon immersion. The open-circuit potential transient in NaOH was measured to obtain corroborating evidence for this result. Two such transients from different experiments are shown in Fig. 15. The curve plotted on a logarithmic time scale illustrates the early portion of the transient, and other measurement shows the trend at later times. Upon immersion, the potential decreases very rapidly to a minimum at about 10 s, then increases to a peak at 20-30 s, and finally decays more slowly to an approximately steady value which is reached at about 100 s. The short-time transient shows that the early decay upon immersion is very rapid. In fact, the ''initial'' potential upon first contact with NaOH cannot be measured effectively, and is possibly near −1.0 V *vs.* SCE, the open-circuit potential of the as-received foil in neutral solution. As the conduction current through the oxide film is a very sensitive function of the electric field, the field in the oxide is frequently found to be roughly constant. Thus, the high speed of the initial potential decay likely reflects rapid film dissolution in the first 1 s, and the fairly constant potential thereafter is associated with a steady-state film thickness. This time dependence of the oxide thickness agrees with that inferred from positron measurements. Both results suggest that changes in the film thickness do not occur at times longer than 10 s,

at which formation of interfacial voids is first apparent. Thus void generation is correlated with metal as opposed to oxide dissolution.

Comments on void formation mechanism.—While it is clear that interfacial voids result from metal dissolution in NaOH, the time when they form is open to question. If voids were created at some time during NaOH immersion, continuing dissolution at later times would eventually expose them at the foil surface. In this case, the presence of cavities in the AFM images in Fig. 9 would be expected. Since none of these images show the presence of cavities similar to the ones in Fig. 10 and 11, void formation during dissolution is difficult to understand. Even if voids are initially only a few nanometers in size, they should be enlarged by dissolution when exposed, and would then probably be detectable with AFM. An alternative mechanism is that voids result from the ''condensation'' of metal vacancies generated at the metal-film interface during the dissolution process. The growth of the voids would then occur by solid-state vacancy diffusion, at times after the NaOH treatment. No surface cavities would then be expected after the treatment. Doherty and Davis observed voids at the aluminum metal-oxide interface after cooling from high temperature.[23,24] These voids were shown to be formed by condensation of thermal vacancies. In the present experiments, the vacancies which condense as voids would be formed by metal atom oxidation during dissolution, by a mechanism whose details are not yet clear. Vacancy condensation would presumably occur either at the metal-film interface itself, or at subsurface nucleation sites such as dislocations. Both types of void sites were suggested above.

The presence of bulk metallic impurities such as lead, even at concentrations as low as 1 ppm, significantly affects the distribution of pits formed during anodic etching.[25] Since the present results suggest that interfacial voids can serve as pit sites, the possibility that impurities play a role in void formation might be considered. Wu and Hebert used Rutherford backscattering spectrometry (RBS) to analyze the surface composition of foils after 1 M NaOH treatment.[9] The concentrations of iron, copper, and gallium accumulated at a constant rate during the treatment, within a layer no thicker than about 10 nm adjacent to the metal-oxide interface. Significant concentration increases were noted after 5 min dissolution. Near-surface accumulations of other impurities such as lead, not detected by RBS, may also have occurred. The impurity buildup at the surface found by Wu occurs more slowly than the formation of the voids, which were detected as early as 10 s (Fig. 1). However, the buildup time of 5 min seems to correspond to the appearance of the scalloped surface topography, along with the particular cavity morphology in Fig. 10 characteristic of dissolution times longer than 5 min. The presence of significant near-surface impurity concentrations at the same times may suggest the possible role of impurities in the formation of these voids.

Conclusions

High-purity aluminum foils were investigated using PAS, in order to explain the formation of near-surface open-volume defects in these foils during dissolution, and also to explore the connection between the defects and sites where corrosion pits initiate. Al foils were exposed to 1 M NaOH for times between 1 s and 30 min, after which PAS measurements were carried out. According to the fitting results, during the first 1 min in NaOH, the defect layer *S* parameter increases from 1.028 to the large value of 1.066, and then slowly decreases. The *S*-*W* plot shows that there is only one defect type on all samples, namely, a metallic void at least of nanometer size and located near the metal-oxide film interface. The high *S* parameter suggests that internal metallic surface of this void either has only a monolayer-thick oxide, or no oxide at all. The time-dependence of the defect layer *S* parameter indicates that defects are formed continuously during dissolution of the metal in NaOH.

The foil surfaces were also examined by AFM after NaOH dissolution. Images were compiled both before and after stripping the surface oxide layer in Cr_2O_3-H_3PO_4 solution at 85°C for 1 min. Images of the surfaces after but not before stripping reveal cavities with depths ranging from 20 to 140 nm, the number, distribution, and shape of which varies significantly with NaOH dissolution time. The mean cavity depth agrees quantitatively at different dissolution times with the defect layer thickness obtained by PAS, and the variation of the total cavity volume with time is nearly the same as that of the defect layer *S* parameter. This evidence suggests that the cavities are interfacial voids formed along with the voids detected by PAS, and are revealed in AFM by dissolution of the overlying oxide. Cavities on as-received foil are found mainly along ridges parallel to the rolling direction, while those on NaOH treated foils are smaller and more evenly distributed on the surface. These distributions resemble closely those of corrosion pits produced by anodic etching in HCl, and the cavity size is similar to those of pits previously observed after millisecond duration etching experiments. Pits are believed to be initiated by dissolution of the oxide above interfacial voids, which exposes their reactive internal surfaces.

Acknowledgments

Support for this work was provided by the National Science Foundation under grant DMR-9307308, and by St. Jude Medical. Aluminum foils were provided by KDK Corporation (Takahagi, Japan). One of us (K.R.H.) is indebted to Bent Nielsen (Brookhaven National Laboratory) and Palakkal Asoka-Kumar (Lawrence Livermore National Laboratory), for many helpful discussions about positron measurements and their interpretation.

Iowa State University assisted in meeting the publication costs of this article.

References

1. P. J. Schultz and K. G. Lynn, *Rev. Mod. Phys.*, **60**, 701 (1988).
2. P. Asoka-Kumar, K. G. Lynn, and D. O. Welch, *J. Appl. Phys.*, **76**, 4935 (1994).
3. P. Hautojärvi and C. Corbel, in *Positron Spectroscopy of Solids*, A. Dupasquier and A. P. Mills, Jr., Editors, p. 491, IOS Press, Amsterdam (1995).
4. X. Wu, K. R. Hebert, P. Asoka-Kumar, and K. G. Lynn, *J. Electrochem. Soc.*, **141**, 3361 (1994).
5. M. Fomino, K. R. Hebert, P. Asoka-Kumar, and K. G. Lynn, in *Critical Factors in Localized Corrosion III*, R. G. Kelly, G. S. Frankel, P. M. Natishan, and R. C. Newman, Editors, PV 98-17, p. 642, The Electrochemical Society Proceedings Series, Pennington, NJ (1999).
6. K. G. Lynn and H. Lutz, *Rev. Sci. Instrum.*, **51**, 977 (1980).
7. M. Fomino, M.S. Thesis, Iowa State University, Ames, IA (1996).
8. T. van Hoecke, D. Segers, H. Schut, C. Dauwe, A. van Veen, B. van Waeyenberge, and L. Palffy, *Mater. Sci. Forum*, **255-257**, 724 (1997).
9. X. Wu and K. R. Hebert, *J. Electrochem. Soc.*, **143**, 83 (1996).
10. P. J. Simpson, P. J. Schultz, T. E. Jackman, G. C. Aers, J.-P. Nöel, D. C. Houghton, D. D. Perovic, and G. C. Weatherly, in *Positron Beams for Solids and Surfaces*, AIP Conference Proceedings, Vol. 218, p. 125, American Institute of Physics (1990).
11. K. G. Lynn and P. J. Schultz, *Appl. Phys. A: Solids Surf.*, **37**, 31 (1985).
12. H. Huomo, E. Soininen, and A. Vehanen, *Appl. Phys. A: Solids Surf.*, **49**, 647 (1989).
13. A. van Veen, H. Schut, and P. E. Mijnarends, in *Positron Beams and Their Applications*, P. G. Coleman, Editor, p. 191, World Publishing Co., Singapore (2000).
14. R. H. Howell, M. Tuomisaari, and Y. C. Jean, *Phys. Rev. B* **42**, 6921 (1990).
15. A. van Veen, H. Schut, J. de Vries, R. A. Hakvoort, and M. R. Ijpma, in *Positron Beams for Solids and Surfaces*, AIP Conference Proceedings, Vol. 218, p. 171, American Institute of Physics (1990).
16. A. van Veen, H. Schut, M. Clement, J. M. M. de Nijs, A. Kruseman, and M. R. Ijpma, *Appl. Surf. Sci.*, **85**, 216 (1995).
17. R. M. Nieminen and M. J. Manninen, in *Positrons in Solids*, P. Hautojärvi, Editor, p. 178, Springer-Verlag, Berlin (1979).
18. J. Scherer, O. M. Magnussen, T. Ebel, and R. J. Behm, *Corros. Sci.*, **41**, 35 (1998).
19. T. Martin and K. R. Hebert, *J. Electrochem. Soc.*, **148**, B101 (2001).
20. E. A. Culpan and D. J. Arrowsmith, *Trans. Inst. Met. Finish.*, **51**, 17 (1973).
21. F. B. Cuff and N. J. Grant, *J. Inst. Met.*, **87**, 248 (1958-59).
22. B. J. Wiersma and K. R. Hebert, *J. Electrochem. Soc.*, **138**, 48 (1991).
23. P. E. Doherty and R. S. Davis, *Acta Metall.*, **7**, 118 (1959).
24. P. E. Doherty and R. S. Davis, *J. Appl. Phys.*, **34**, 619 (1963).
25. Z. Ashitaka, G. E. Thompson, P. Skeldon, G. C. Wood, H. Habazaki, and K. Shimizu, *J. Electrochem. Soc.*, **147**, 132 (2000).